

## Article

# Mechanical and Durability Properties of Cementless Concretes Made Using Three Types of CaO-Activated GGBFS Binders

Woo Sung Yum, Juan Yu, Dongho Jeon , Haemin Song, Sungwon Sim, Do Hoon Kim and Jae Eun Oh \* 

School of Urban and Environmental Engineering, Ulsan National Institute of Science and Technology (UNIST), UNIST-gil 50, Ulsu-gun, Ulsan 44919, Korea; reikoku@nate.com (W.S.Y.); cp9eins@unist.ac.kr (J.Y.); dhjeon0707@gmail.com (D.J.); haemin93@unist.ac.kr (H.S.); conor123@naver.com (S.S.); elvis03@unist.ac.kr (D.H.K.)

\* Correspondence: ohjaeeun@unist.ac.kr

**Abstract:** This study examined the mechanical and durability properties of CaO-activated ground-granulated blast-furnace slag (GGBFS) concretes made with three different additives ( $\text{CaCl}_2$ ,  $\text{Ca}(\text{HCOO})_2$ , and  $\text{Ca}(\text{NO}_3)_2$ ) and compared their properties to the concrete made with 100% Ordinary Portland Cement (OPC). All concrete mixtures satisfied targeted air content and slump ranges but exhibited significantly different mechanical and durability properties. The CaO-activated GGBFS concretes showed different strength levels, depending on the type of additive. The added  $\text{CaCl}_2$  was the most effective, but  $\text{Ca}(\text{NO}_3)_2$  was the least effective at increasing mechanical strength in the CaO-activated GGBFS system. The OPC concrete showed the most excellent freezing–thawing resistance in the durability test, but only the CaO-activated GGBFS concrete with  $\text{CaCl}_2$  exhibited relatively similar resistance. In addition, the chemical resistance was significantly dependent on the type of acid solution and the type of binder. The OPC concrete had the best resistance in the HCl solution, while all CaO-activated GGBFS concretes had relatively low resistances. However, in the  $\text{H}_2\text{SO}_4$  solution, all CaO-activated GGBFS concretes had better resistance than the OPC concrete. All concrete with sulfate ions had ettringite before immersion. However, when they were immersed in HCl solution, ettringite tended to decrease, and gypsum was generated. Meanwhile, the CaO-activated GGBFS concrete with  $\text{CaCl}_2$  did not change the type of reaction product, possibly due to the absence of ettringite and  $\text{Ca}(\text{OH})_2$ . When immersed in an  $\text{H}_2\text{SO}_4$  solution, ettringite decreased, and gypsum increased in all concrete. In addition, the CaO-activated concrete with  $\text{CaCl}_2$  had a considerable amount of gypsum; it seemed that the dissolved C-S-H and calcite, due to the low pH, likely produced  $\text{Ca}^{2+}$  ions, and gypsum formed from the reaction between  $\text{Ca}^{2+}$  and  $\text{H}_2\text{SO}_4$ .

**Keywords:** CaO-activation; auxiliary activator; GGBFS; chemical resistance; freezing; thawing



**Citation:** Yum, W.S.; Yu, J.; Jeon, D.; Song, H.; Sim, S.; Kim, D.H.; Oh, J.E. Mechanical and Durability Properties of Cementless Concretes Made Using Three Types of CaO-Activated GGBFS Binders. *Materials* **2022**, *15*, 271. <https://doi.org/10.3390/ma15010271>

Academic Editor: Jean-Marc Tulliani

Received: 8 November 2021

Accepted: 28 December 2021

Published: 30 December 2021

**Publisher's Note:** MDPI stays neutral with regard to jurisdictional claims in published maps and institutional affiliations.



**Copyright:** © 2021 by the authors. Licensee MDPI, Basel, Switzerland. This article is an open access article distributed under the terms and conditions of the Creative Commons Attribution (CC BY) license (<https://creativecommons.org/licenses/by/4.0/>).

## 1. Introduction

With global warming, abnormal climates are occurring worldwide, causing many problems [1,2]. The international community agreed to reduce greenhouse gas emissions through the Paris Climate Agreement, to prevent accelerating global warming.

There is increasing demand for materials to replace Portland cement [3,4] because the OPC industry accounts for 8 to 10% of worldwide  $\text{CO}_2$  emissions, accelerating global warming [5]. Therefore, many studies have been conducted on developing alternative binders with a low carbon footprint, using various industrial by-products, such as fly ash or ground-granulated blast-furnace slag (GGBFS) to replace OPC [6–8]. Fly ash-based geopolymers using fly ash as the main material use alkaline activators, such as sodium hydroxide (NaOH), potassium hydroxide (KOH), or sodium silicates (e.g., water glass). Palomo et al. [9] reported that geopolymer activated with NaOH 8–12 M cured at 85 °C showed a compressive strength of about 40 MPa, and it reached nearly 90 MPa when water glass was added to the binder. Sun et al. [10] explored the effect of three different aggregate sizes on the strength of geopolymers. M.A.M Ariffin et al. [11] showed that geopolymer concrete exhibited better sulfuric

acid resistance than OPC concrete. Although geopolymer has high compressive strength and durability, it has the disadvantage that its performance changes depending on the type of activator and curing temperature [12]. Furthermore, U Yurt et al. [13] showed the performance of alkali-activated GGBFS composite varying with the different alkali activators and activation temperature. In addition, many studies [14,15] reported that alkaline activated GGBFS binders have high compressive strength and chemical resistance. However, similar to geopolymers, GGBFS-based cementless binders have drawbacks in the following usages [16]: (1) high material costs, (2) user safety, and (3) difficulty in producing a one-part binder. Despite these problems, alkali-activated binders produce comparable mechanical properties compared to the OPC binder [17,18]; thus, many studies have been conducted at the concrete level to validate the mechanical and durability properties [19,20].

On the other hand, the CaO-activated binder system [21,22] relatively overcame the disadvantages mentioned above of alkali-activated binders. Kim et al. [23] studied CaO-activated GGBFS binder, and Yum et al. [21,24,25] enhanced mechanical properties of CaO-activated GGBFS binders by adding different types of additional activators. In addition, there are studies to develop cementless binders by activating fly ash using CaO and other chemical additives [22,26]. Although the CaO-activated binders can potentially apply to construction fields, no study has been conducted at the concrete level on mechanical properties and durability.

Therefore, this study compared the mechanical and durability properties of various CaO-activated GGBFS concretes using additives,  $\text{CaCl}_2$ ,  $\text{Ca}(\text{HCOO})_2$ , and  $\text{Ca}(\text{NO}_3)_2$ . Mechanical properties, such as compressive strength, tensile splitting strength, and elastic modulus were measured. In addition, the durability properties were evaluated by the freezing and thawing cycle test and the chemical resistance test using hydrochloric acid (HCl) and sulfuric acid ( $\text{H}_2\text{SO}_4$ ). Changes in hydration products were examined through powder X-ray diffraction (XRD) measurement and thermogravimetry analysis (TGA).

## 2. Materials and Methods

Commercial OPC (type I, 42.5N) and GGBFS were used in this study. In addition, all used chemicals were analytical grade. CaO (Daejung, Korea) was the main activator, and  $\text{CaCl}_2$  (Daejung, Korea),  $\text{Ca}(\text{HCOO})_2$  (Aladdin, China),  $\text{Ca}(\text{NO}_3)_2$  (Sigma Aldrich, Burlington, MA, USA), and  $\text{CaSO}_4$  (Daejung, Korea) were additives. The maximum size of coarse aggregate was 25 mm. Fine aggregate were classified as aggregates with a size less than 5 mm. All aggregates were used under saturated surface dry (SSD) conditions. In addition, a naphthalene-based commercial plasticizer was used in concrete mixtures.

XRD, XRF, and particle size distribution analysis were performed to identify the characteristics of the raw materials (i.e., OPC and GGBFS). XRD patterns were recorded by means of a D/Max2500 V diffractometer (Rigaku, Japan) with an incident beam of  $\text{Cu-K}\alpha$  radiation ( $\lambda = 1.5418 \text{ nm}$ ) in a  $2\theta$  scanning range from  $5^\circ$  to  $60^\circ$ ; X-ray fluorescence was conducted with S8-Tiger spectrometer (Bruker, Billerica, MA, USA).

Particle size distribution results (Figure 1) show that the average particle sizes of OPC and GGBFS were 25 and 30  $\mu\text{m}$ , respectively. Table 1 exhibits the XRF results of OPC and GGBFS, and they mainly consisted of CaO and  $\text{SiO}_2$ . In Figure 2, the XRD results show that akermanite [ $\text{Ca}_2\text{Mg}(\text{Si}_2\text{O}_7)$ ] was identified in GGBFS, and GGBFS primarily consisted of an amorphous phase. On the other hand, dicalcium silicate ( $\text{C}_2\text{S}$ ), tricalcium silicate ( $\text{C}_3\text{S}$ ), tetracalcium aluminoferrite ( $\text{C}_4\text{AF}$ ), tricalcium aluminate ( $\text{C}_3\text{A}$ ), and gypsum ( $\text{CaSO}_4$ ) were identified in OPC [27].

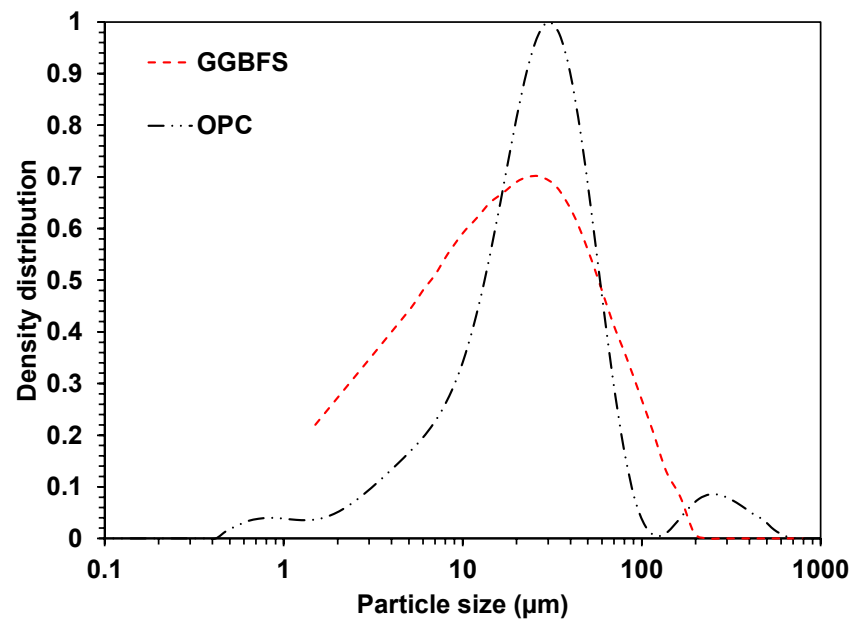


Figure 1. Particle size distributions of OPC and GGBFS.

Table 1. Oxide compositions: OPC and GGBFS (wt%).

Oxide	OPC	GGBFS
CaO	64.05	59.48
SiO <sub>2</sub>	18.59	23.05
Al <sub>2</sub> O <sub>3</sub>	4.45	9.72
MgO	3.14	2.54
SO <sub>3</sub>	3.55	1.37
TiO <sub>2</sub>	0.29	0.98
MnO	0.19	0.83
Fe <sub>x</sub> O <sub>y</sub>	3.61	0.68
K <sub>2</sub> O	1.23	0.68
Na <sub>2</sub> O	0.29	0.28
Others	0.61	0.4

Table 2. Material proportions of binders used in concrete mixture samples (wt%).

Binder Type	OPC	GGBFS	CaO	CaCl <sub>2</sub>	Ca(HCOO) <sub>2</sub>	Ca(NO <sub>3</sub> ) <sub>2</sub>	CaSO <sub>4</sub>	Sum
P-binder	100	0	0	0	0	0	0	100
C-binder	0	94	4	2	0	0	0	100
F-binder	0	88	4	0	3	0	5	100
N-binder	0	86	4	0	0	5	5	100

The material proportions of binders used to produce concrete samples are shown in Table 2. The P-binder was 100% OPC. The other binders (C-, F-, and N-binders) were CaO-activated GGBFS binders, which used CaO as a primary activator for activating GGBFS while included different additives. The C-binder, F-binder, and N-binder used CaCl<sub>2</sub>, Ca(HCOO)<sub>2</sub>, and Ca(NO<sub>3</sub>)<sub>2</sub>, respectively, as additives, and their material proportions were determined via previous studies [21,24,25]. Note that F-binder and N-binder additionally

used five weight percentages of  $\text{CaSO}_4$  to enhance the early compressive strength of the binders.

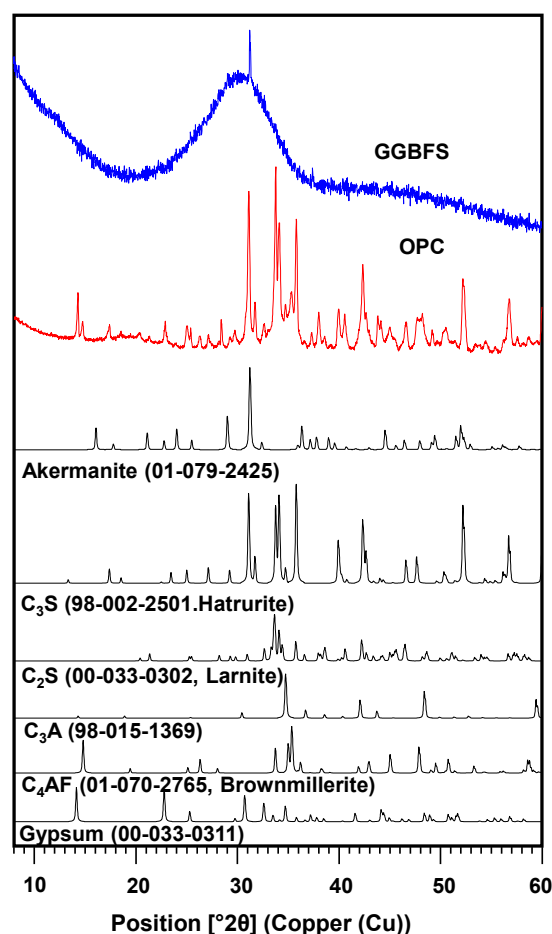


Figure 2. XRD patterns of OPC and GGBFS with identified phases.

The mixture proportions of concrete are given in Table 3, and the samples were labeled similarly after the used binders. According to the Korea Concrete Specification [28], concrete mixture proportions were designed, and the targeted compressive strength was above 45 MPa. Targeted slump and air content ranges were 5–15 cm and 3–6%, respectively.

Table 3. Mixture proportions of concrete samples.

Sample	Binder Type	$G_{\max}$ (mm)	w/b (wt%)	s/a (vol%)	Unit Weight ( $\text{kg}/\text{m}^3$ )				
					Water	Binder	FA	CA	Plasticizer
P-CON	P-binder	25	36.73	42.31	176.63	480.82	687.81	955.86	0.14
C-CON	C-binder						676.34	939.93	0.14
F-CON	F-binder						673.87	936.48	0.14
N-CON	N-binder						673.87	936.48	0.14

Note: FA denotes fine aggregate; CA denotes coarse aggregate;  $G_{\max}$  denotes the ratios of the maximum size of coarse aggregate; w/b denotes water to binder weight ratio, and s/a denotes sand to aggregate volume.

For concrete production, all mixing procedures followed the Korea Standard (KS) F 2403 [29]. The fresh concrete samples were cast in cylindrical molds ( $\varnothing 10 \text{ cm} \times 20 \text{ cm}^3$ ) to test determine compressive strength, split strength, elastic modulus, and chemical resistance, and samples in prism molds ( $10 \times 10 \times 40 \text{ cm}^3$ ) for freezing and thawing

cycle tests. The fresh concrete samples were compacted and cured at 23 °C and 99% relative humidity.

Slump and air content were examined according to the KS F 2402 and KS F 2421 [30,31]. The slump and air content tests were conducted once for each mixture proportion. Triplicate samples were tested for compressive and split strength of each mixture at 3, 7, and 28 days of curing. Chord elastic modulus was measured for the 28-day cured samples, and triplicate specimens were tested for each mixture. The elastic modulus was calculated using the chord modulus using stress-strain curves obtained from three linear variable differential transformers (LVDT) installed in longitudinal directions of concrete [27]. The measured elastic modulus was compared with models proposed by the American Concrete Institute (ACI) 318 and the Euro-International Committee for Concrete—the International Federation for Pre-stressing (CEB-FIP); the CEP-FIP equations are as follows [32,33]:

$$\text{ACI Model : } E_c = W_c^{1.5} \times 0.043 \sqrt{f_{28}}$$

$$\text{CEB - FIP : } E_c = 2.15 \times 10^4 \left( \frac{f_{28}}{10} \right)^{1/3}$$

where  $E_c$  is the elastic modulus (GPa),  $f_{28}$  is the 28-day compressive strength (MPa), and  $w_c$  is density ( $\text{kg/m}^3$ ).

Freezing and thawing cycle resistance tests were performed using 14-day cured samples, and all experimental procedures followed by KS F 2456 [34]. In addition, three identical samples were used on each measurement date. The initial weight and dynamic modulus of elasticity were recorded for 14 days after curing, and then the samples were tested for freezing and thawing cycles. Each cycle consisted of  $-20$  °C to  $4$  °C; the time of each cycle was less than 4 h, and the relative dynamic modulus of elasticity and weight change were measured every 30 cycles. Three identical samples were used for each concrete, and the experiments were conducted up to 300 cycles.

Chemical resistance tests were carried out according to ASTM C 267 [35]. The 28-day cured samples were immersed in a container with 5% HCl and 5%  $\text{H}_2\text{SO}_4$  solutions, and the solutions were replaced once in 4 weeks. The weight changes were measured at 3, 7, 14, 28, 56, and 91 days after immersion to identify the evolution of reaction products. On each weight measurement, three identical specimens were weighed. Analysis of XRD and TGA identified reaction products after 28, 56, and 91 days of immersion. The exposed samples were fractured and finely ground using a mortar and pestle. In addition, XRD and TGA were conducted once for each measurement day and mixture proportion. In addition, SDT Q600 (TA Instruments, New Castle, DE, USA) was used to measure the reaction products of each sample with a heating rate of  $30$  °C/min from  $25$  to  $1000$  °C in a nitrogen atmosphere in an alumina pan.

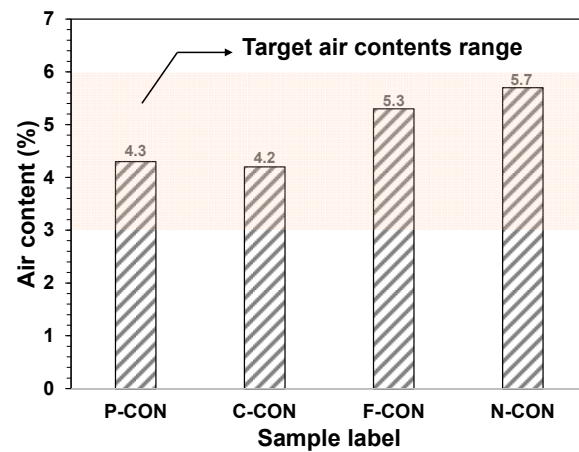
### 3. Results

#### 3.1. Slump and Air Content

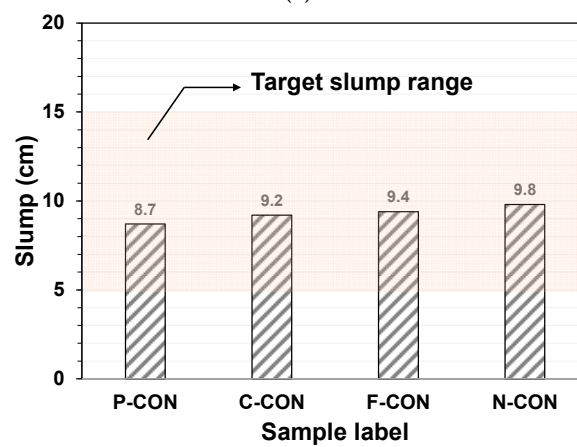
Figure 3 displays the air content and slump measurement test results. The air content and the slump values satisfied the criteria specified in KS F 2421 (air content = 3–6%) and KS F 2402 (slump = 5–15 cm) [30,31], respectively.

#### 3.2. Compressive and Split Strength

Compressive strengths of hardened concretes are shown in Figure 4, and the greatest compressive strength was measured from P-CON at all curing days. In addition, all mixtures showed increased strengths with increasing curing days. All cementless concrete samples exhibited significantly lower compressive strengths than P-CON at three days, mainly due to the lower reaction rate of CaO-activated GGBFS binders than OPC binder [36]. The type of used additives influenced the strength development of CaO-activated GGBFS concretes.  $\text{CaCl}_2$  was the most effective in increasing strength, while  $\text{Ca}(\text{NO}_3)_2$  was the least effective.



(a)



(b)

Figure 3. The test results: (a) air content and (b) slump of fresh concrete samples.

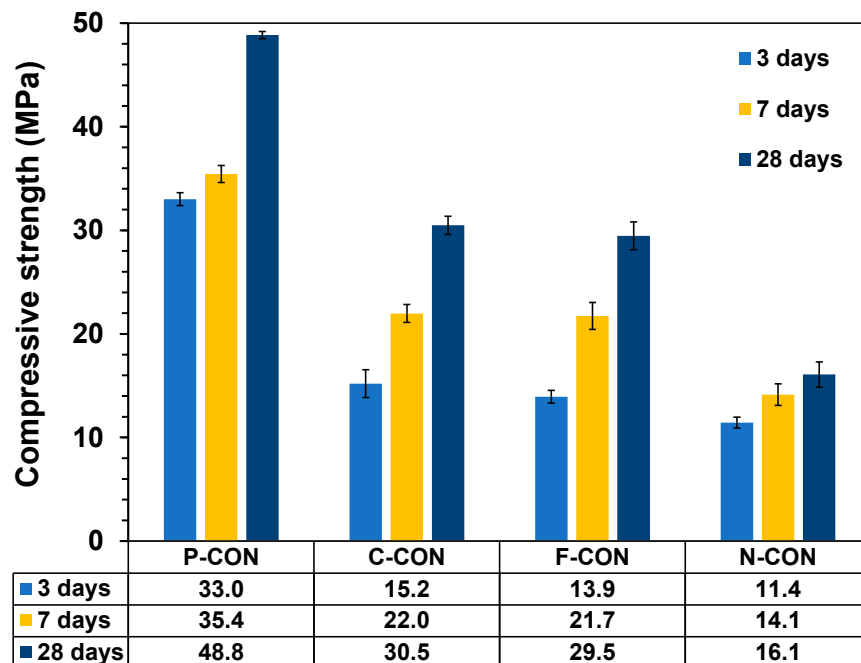


Figure 4. Compressive strengths of hardened concrete samples.

The mixture proportion of concrete was designed following the Concrete Standard Specification in Korea [37], and the designed 28-day compressive strength ( $f_{cr}$ ) was 45 MPa. The compressive strength was 48 MPa for P-CON, but the CaO-activated GGBFS concretes gained only about 10 to 30 MPa, significantly lower compressive strength than  $f_{cr}$ .

The split strengths are presented in Figure 5. The tensile strength of OPC concrete was reported as about 10 to 15% of the compressive strength [27]. The concrete specimens made with CaO-activated GGBFS binders having no OPC also exhibited a similar trend in this study.

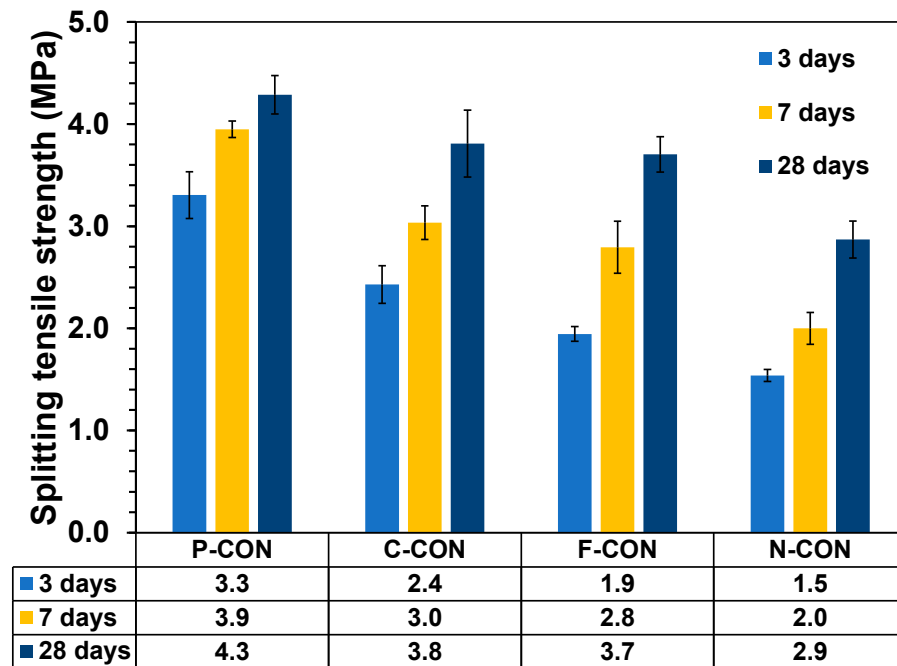


Figure 5. Split strengths of hardened concrete samples.

### 3.3. Chord Elastic Modulus

The measured elastic modulus values of concrete samples are given in Table 4 with the calculated values from ACI 318 and CEB-FIP model codes. It is known that the strength and elastic modulus had a proportional relationship in OPC concrete [27], and the same tendency was observed for all binder types of concrete in this study.

Table 4. The results of elastic modulus using experiments and model codes.

Sample Label	Compressive Strength at 28 Days (MPa)	Density (kg/m <sup>3</sup> )	Elastic Modulus (GPa)		
			Exp.	ACI 318	CEB-FIP
P-CON	44.8	2415.5	28.8	34.1	41.5
C-CON	30.5	2372.6	20.9	27.4	35.7
F-CON	29.5	2349.7	19.1	26.6	34.7
N-CON	20.7	2360.2	17.2	19.7	29.1

When comparing the experimental values with the calculated values from the ACI and CEB-FIP models, the models showed significantly higher elastic modulus than the measured values. Previous studies similarly reported that the ACI and CEB-FIP models tended to overestimate the elastic modulus of OPC concrete, and it was observed for all types of concretes in this study [38–40].

### 3.4. Freezing and Thawing Cycle Tests

Figure 6 presents the freezing and thawing cycle test results for changing relative dynamic modulus of elasticity and weight loss with increasing cycles.

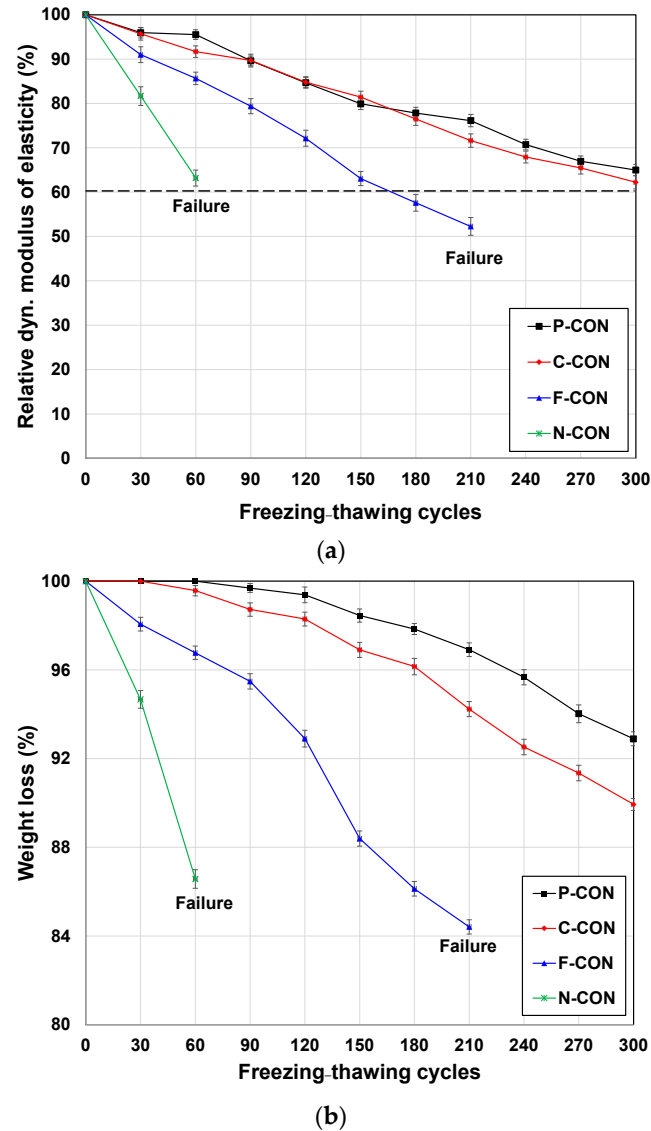


Figure 6. Freezing and thawing test results: (a) relative dynamic modulus of elasticity and (b) weight loss.

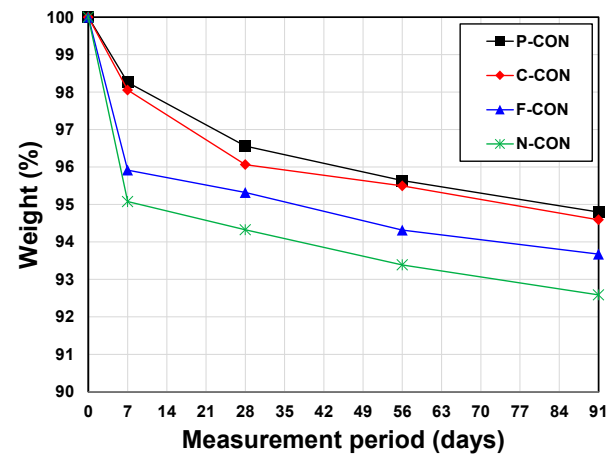
The dynamic elastic modulus of P-CON and C-CON decreased down to about 60% up to 300 cycles, while those of F-CON and N-CON were not measured because they were damaged significantly before reaching 300 cycles. Thus, F-CON and N-CON are vulnerable to freezing and thawing cycles.

It is worth noting that although C-CON and F-CON had similar compressive strengths and elastic modulus, they showed significantly different resistances to freezing and thawing cycles. However, a sample with a higher drop of the dynamic modulus tended to show a steeper decrease in the weight. Thus, the strength itself was a less accurate indicator than the dynamic modulus for estimating the ability to resist freezing and thawing cycles in this study.

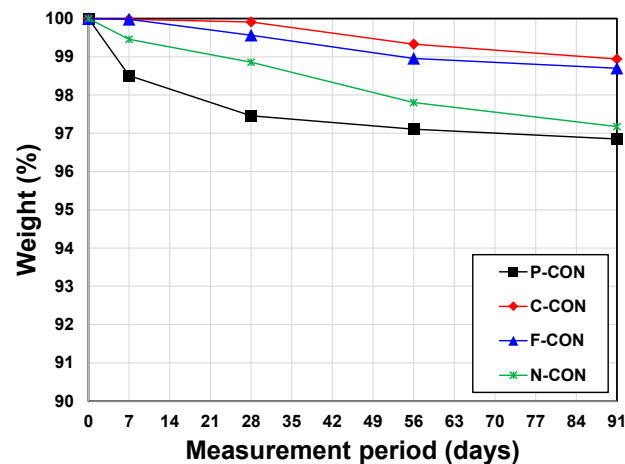
For OPC concretes, KS F 2456 [34] determines that OPC concrete is susceptible to freezing and thawing cycles when OPC concrete samples are destroyed before 300 cycles or when the dynamic elastic modulus decreases below 60% after 300 cycles. Thus, this study implies that KS F 2456 can also be applied to the CaO-activated GGBFS system.

### 3.5. Chemical Resistance Tests (5% HCl and 5% H<sub>2</sub>SO<sub>4</sub>)

The results of chemical resistance tests using 5% HCl and 5% H<sub>2</sub>SO<sub>4</sub> solutions are shown in Figure 7. Significantly different results were obtained, depending on the type of solutions. In 5% HCl aqueous solutions, although weight loss was observed in all immersed samples, P-CON had the most excellent resistance, while N-CON was the most vulnerable. However, the samples immersed in 5% H<sub>2</sub>SO<sub>4</sub> aqueous solutions yielded different results; the most considerable weight loss occurred in P-CON, followed by N-CON, F-CON, and C-CON, in order.



(a)



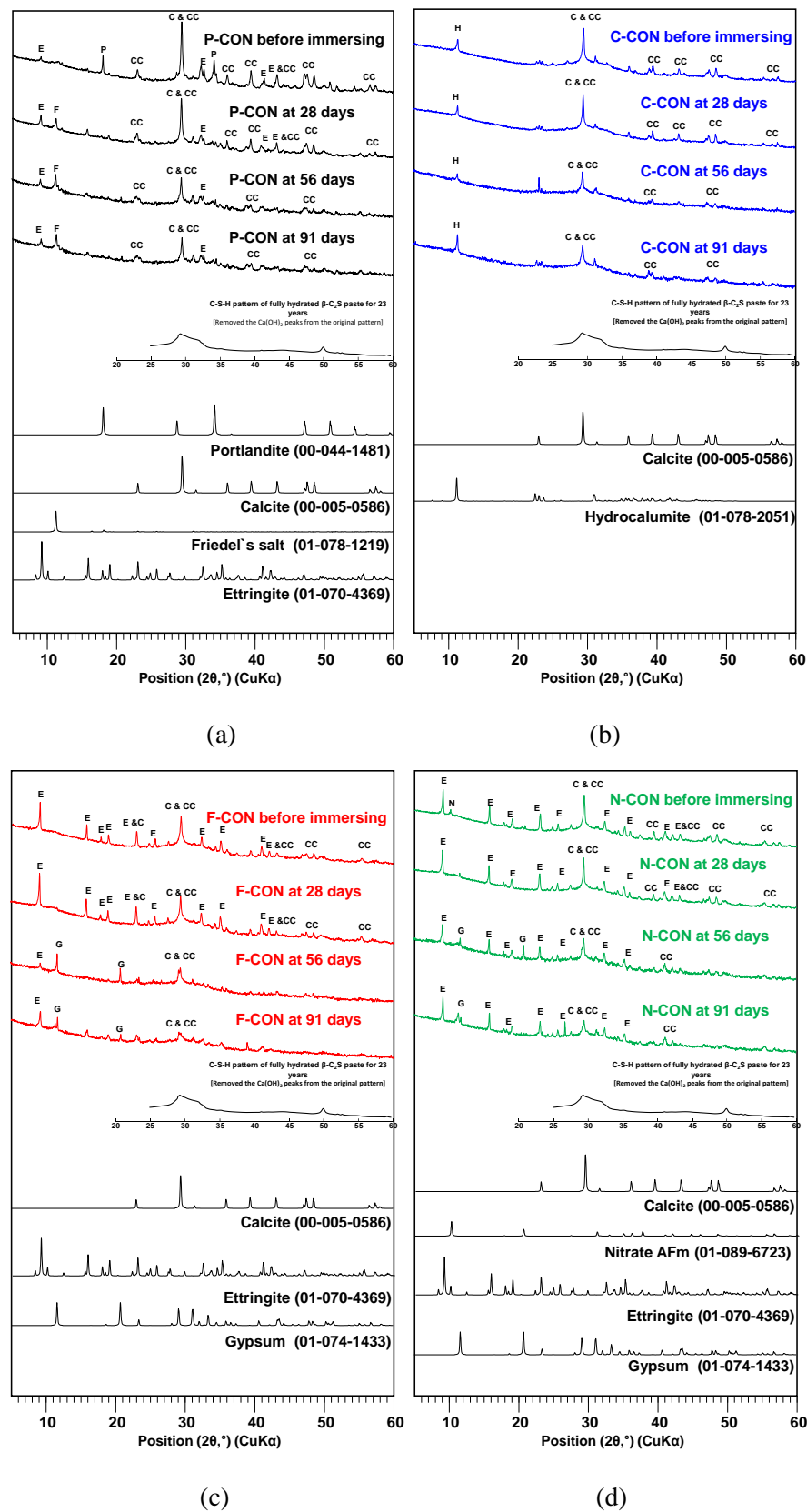
(b)

Figure 7. Chemical resistance test results: (a) 5% HCl solution and (b) 5% H<sub>2</sub>SO<sub>4</sub> solution.

### XRD and TG/DTG Analysis in Chemical Resistance Tests

When concrete samples were immersed in acid solutions (i.e., HCl and H<sub>2</sub>SO<sub>4</sub>), the pH of the concrete was lowered, resulting in the change of hydration products.

In the HCl solution, the change of the reaction products was investigated using the XRD and TG/DTG analysis, shown in Figures 8 and 9, respectively. After immersion, Ca(OH)<sub>2</sub> disappeared in the P-CON sample, and Friedel's salt (Ca<sub>2</sub>Al(OH)<sub>6</sub>Cl(H<sub>2</sub>O)<sub>2</sub>) was found. The HCl solution likely lowered the pH of P-CON, resulting in removing OH<sup>-</sup> of Ca(OH)<sub>2</sub> [41,42], and Friedel's salt was produced by the reaction of Cl<sup>-</sup> ions from HCl and Ca<sup>2+</sup> ions from Ca(OH)<sub>2</sub>. In addition, regeneration of Ca(OH)<sub>2</sub> was observed at the 91-day sample. It seemed that as the chemical resistance test proceeded, Ca(OH)<sub>2</sub> was regenerated by a complex chemical reaction; more research will likely be needed for the regeneration of Ca(OH)<sub>2</sub>.



**Figure 8.** XRD patterns of hardened samples immersed in 5% HCl solution: (a) P-CON, (b) C-CON, (c) F-CON, and (d) N-CON. (Note. E: ettringite, C: C-S-H, CC: calcite, G: gypsum, H: hydrocalumite, F: Friedel's salt, P: portlandite, and N: nitrate AFm, respectively).

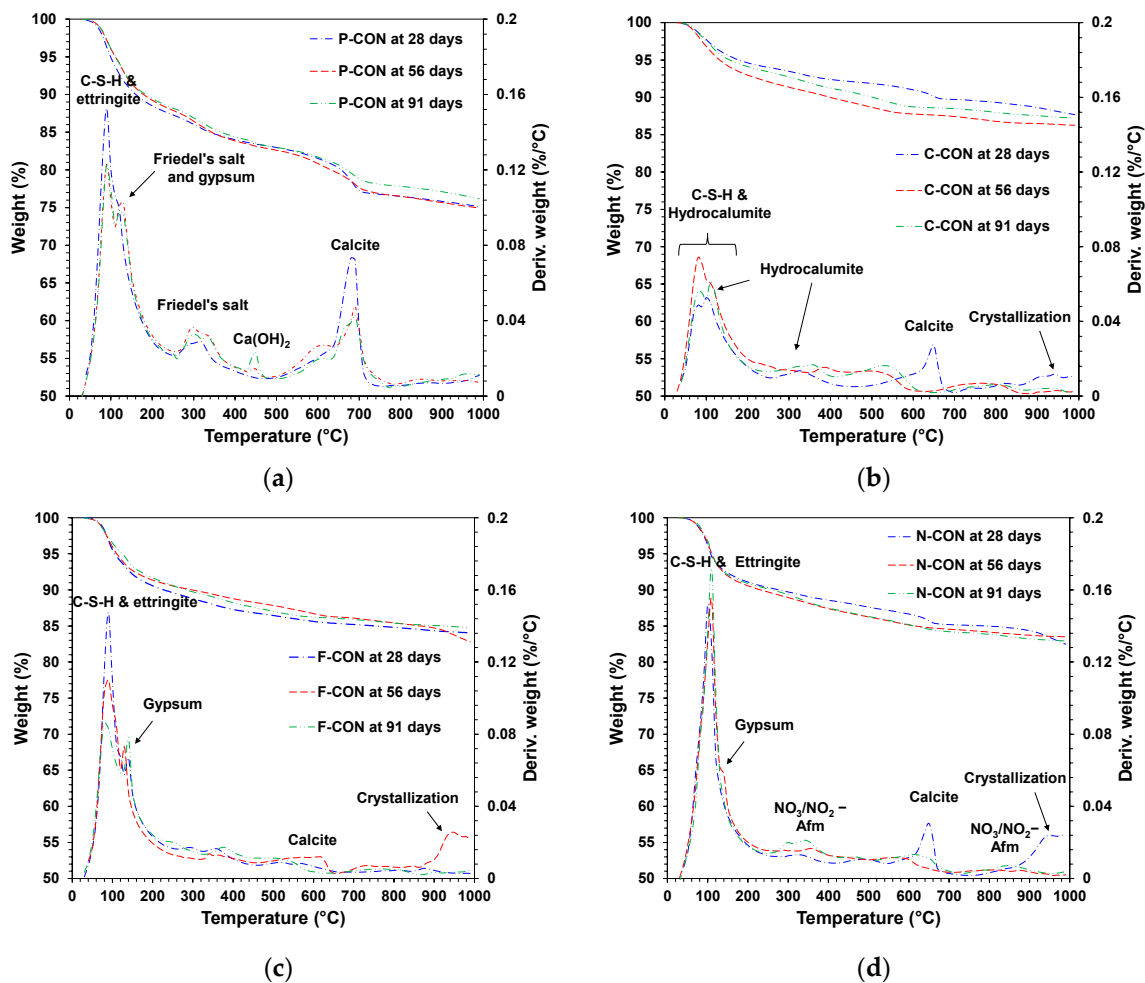


**Figure 9.** TG/DTG curves of hardened samples immersed in 5% HCl solution: (a) P-CON, (b) C-CON, (c) F-CON, and (d) N-CON.

The XRD showed that all samples with sulfate ion ( $\text{SO}_4^{2-}$ ) (i.e., P-, F-, and N-CON) had ettringite before immersion. When immersed in HCl solution, the DTG analysis showed that ettringite tended to decrease, and gypsum was generated; F-CON exhibited the most prominent decrease of ettringite, while N-CON displayed the slightest change in ettringite peak. Previous studies [41,43,44] reported that, below pH value of 10.6, ettringite was no longer stable, and gypsum formed. Unlike the other samples, C-CON did not change the type of reaction product in the HCl solution, possibly due to the absence of ettringite and  $\text{Ca}(\text{OH})_2$  before immersion. In addition, the weight loss occurred in the vicinity of 800 to 900 °C in CaO-activated concrete, which might be the recrystallization of C-S-H [45].

Figures 10 and 11 show the results of XRD and TG/DTG tests, respectively, for the samples in the  $\text{H}_2\text{SO}_4$  solution. In addition, similar to the HCl results, regeneration of  $\text{Ca}(\text{OH})_2$  at the P-CON sample and crystallization were observed. It is worth noting that ettringite is relatively more susceptible to the drying process of sample preparation than other cementitious reaction products and, thus, ettringite can often be underestimated in quantity in XRD and TG/DTG [46,47]. Unfortunately, in this study, the result for ettringite in the  $\text{H}_2\text{SO}_4$  solution in TG/DTG was not precisely consistent with that of XRD; however, careful interpretation enabled us to recognize the approximate tendency of the product change.

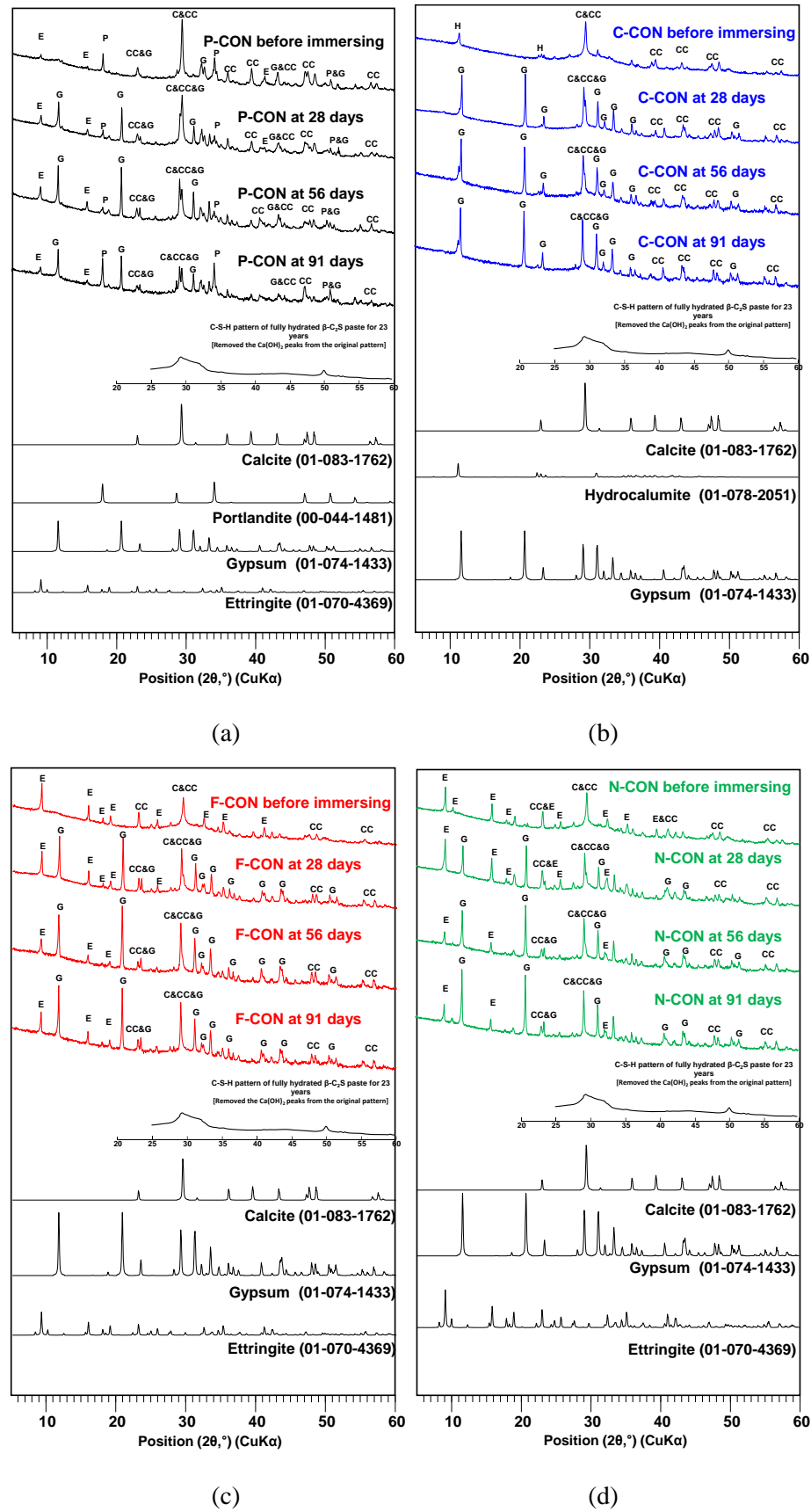


**Figure 10.** XRD patterns of hardened samples immersed in 5% H<sub>2</sub>SO<sub>4</sub> solution: (a) P-CON, (b) C-CON, (c) F-CON, and (d) N-CON. (Note. E: ettringite, C: C-S-H, CC: calcite, G: gypsum, H: hydrocalumite, and P: portlandite, respectively).

In the samples that had ettringite before immersion (i.e., P-, F-, and N-CON in Figure 10), as the DTG peaks of ettringite decreased, the gypsum DTG peaks tended to increase, as shown in Figure 11. In particular, the F-CON and N-CON samples showed relatively strong gypsum XRD and DTG peaks, and the peaks were even stronger than those of samples in the HCl solution. The cause of gypsum formation was similar to the case of HCl immersion; as the pH of the concrete was likely lowered in the  $H_2SO_4$  solution, ettringite became unstable and decomposed, producing gypsum.

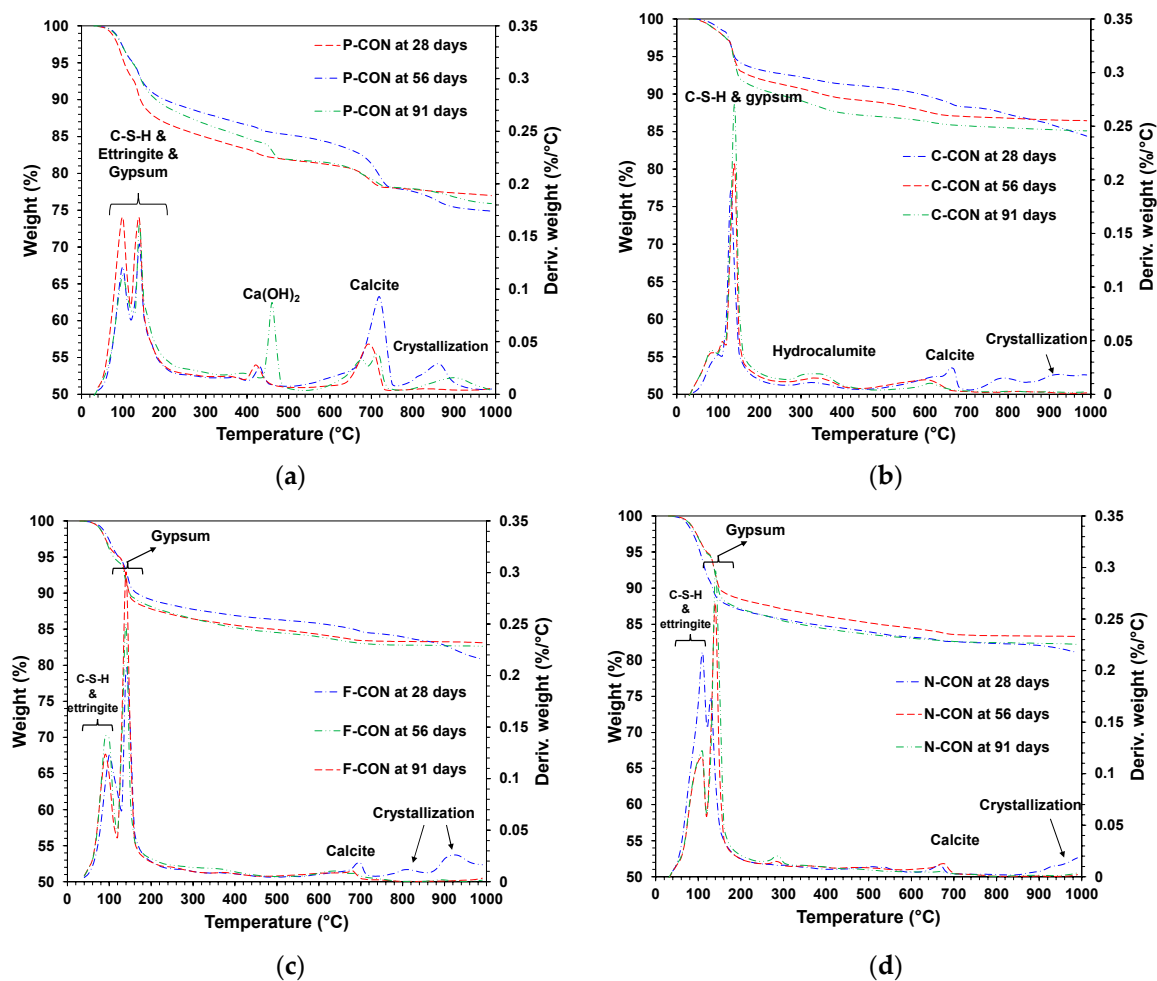


**Figure 11.** TG/DTG curves of hardened samples immersed in 5%  $H_2SO_4$  solution: (a) P-CON, (b) C-CON, (c) F-CON, and (d) N-CON.

However, note that gypsum can also form from the reaction between  $Ca(OH)_2$  and  $H_2SO_4$  without ettringite decomposition [27,41]. For instance, in P-CON, because  $Ca(OH)_2$  was present before immersion, this reaction surely accounted for a portion of gypsum formation. However, this reaction was also likely responsible for the gypsum formation in C-CON despite no  $Ca(OH)_2$  before immersion (Figures 10b and 11b). Previous studies [27,41,48–51] reported that C-S-H and calcite can dissolve, producing  $Ca^{2+}$  ions (or  $Ca(OH)_2$ ) when the pH is lowered. In the TG/DTG results, the decrease in calcite peak was—relatively—clearly seen, but the decrease in C-S-H peak was difficult to observe because the C-S-H peak below 200 °C overlapped with the peaks of ettringite and gypsum, making it challenging to analyze. However, when referring to the other study results [49–51], C-S-H likely dissolved to some extent similar to calcite. Thus, the dissolved  $Ca^{2+}$  ions can produce gypsum from the reaction with  $H_2SO_4$  in C-CON. On the other hand, in the case of P-CON, the coexistence of  $Ca(OH)_2$  generally prevents chemical deterioration of C-S-H [49,52]; thus, a relatively smaller amount of C-S-H likely dissolved than the other samples.

#### 4. Conclusions

This study examined the mechanical and durability properties of three types of CaO-activated GGBFS concretes made with three different additives ( $\text{CaCl}_2$ ,  $\text{Ca}(\text{HCCO})_2$ , and  $\text{Ca}(\text{NO}_3)_2$ ), and compared their properties with those of Portland cement concrete. Detailed conclusions are summarized as follows:

1. All CaO-activated GGBFS concretes satisfied the targeted air content and slump ranges. However, they exhibited lower mechanical properties (compressive strength, split strength, and elastic modulus) than OPC concrete.
2. In the CaO-activated GGBFS system, the additive  $\text{CaCl}_2$  was the most effective at increasing strength and elastic modulus, while the additive  $\text{Ca}(\text{NO}_3)_2$  was the least effective.
3. In the freezing and thawing cycle test, the CaO-activated GGBFS concretes with added  $\text{Ca}(\text{HCCO})_2$  and  $\text{Ca}(\text{NO}_3)_2$  were destroyed before 300 cycles; however, the one made with  $\text{CaCl}_2$  had a relatively comparable resistance in the freezing and thawing cycles test to OPC concrete.
4. The strength was a less accurate indicator than the dynamic modulus for estimating the ability to resist freezing and thawing cycles in this study.
5. The chemical resistance tests using 5% HCl and 5%  $\text{H}_2\text{SO}_4$  solutions showed significantly different results depending on the type of acid solutions. In a 5% HCl solution, although weight loss was observed in all immersed samples, the OPC concrete had the most excellent resistance, while the CaO-activated GGBFS concrete with  $\text{Ca}(\text{NO}_3)_2$  was the most vulnerable. However, in 5%  $\text{H}_2\text{SO}_4$  aqueous, the most considerable weight loss occurred in the OPC concrete.
6. In XRD, all concrete with added sulfate ion ( $\text{SO}_4^{2-}$ ) (i.e., Portland cement concrete and CaO-activated GGBFS concretes with  $\text{Ca}(\text{HCCO})_2$  and  $\text{Ca}(\text{NO}_3)_2$ ) had ettringite before immersion. When they were immersed in HCl solution, their DTG results showed that ettringite tended to decrease, and gypsum was generated; however, the CaO-activated GGBFS concrete with  $\text{CaCl}_2$  did not change the type of reaction product in the HCl solution, possibly due to the absence of ettringite and  $\text{Ca}(\text{OH})_2$  before immersion.
7. When immersed in  $\text{H}_2\text{SO}_4$  solution, similar to the case of HCl, the DTG peaks of ettringite decreased, and the gypsum DTG peaks tended to increase. However, in the  $\text{H}_2\text{SO}_4$  solution, gypsum was synthesized from the reaction between  $\text{Ca}(\text{OH})_2$  and  $\text{H}_2\text{SO}_4$  in all concrete samples. In particular, the concrete without ettringite (i.e., CaO-activated GGBFS concrete with  $\text{CaCl}_2$ ) had a considerable amount of gypsum formation; in this concrete, dissolved C-S-H and calcite, due to the low pH, likely produced  $\text{Ca}^{2+}$  ions, and gypsum formed from the reaction between  $\text{Ca}^{2+}$  and  $\text{H}_2\text{SO}_4$ .

**Author Contributions:** Conceptualization, W.S.Y. and J.Y.; methodology, W.S.Y. and D.J.; software, W.S.Y. and H.S.; investigation, W.S.Y. and S.S.; resources, W.S.Y. and D.H.K.; writing—original draft preparation, W.S.Y. and J.E.O.; writing—review and editing, W.S.Y. and J.E.O.; visualization, W.S.Y. and J.E.O.; supervision, J.E.O.; project administration, J.E.O.; funding acquisition, J.E.O. All authors have read and agreed to the published version of the manuscript.

**Funding:** This research was supported by the Basic Research Program through the National Research Foundation of Korea (NRF) funded by the MSIT (grant number: 2021R1A4A1030867), and Carbon Neutral Institute Project Fund (Project Number: 1.210109.01) of UNIST(Ulsan National Institute of Science & Technology).

**Institutional Review Board Statement:** Not applicable.

**Informed Consent Statement:** Not applicable.

**Data Availability Statement:** Not applicable.

**Conflicts of Interest:** The authors declare no conflict of interest.

## References

1. Kerr, R.A. Global warming is changing the world. *Science* **2007**, *316*, 188–190. [[CrossRef](#)]
2. Drake, F. *Global Warming*; Routledge: Abingdon, UK, 2014.
3. Aitcin, P.-C. Cements of yesterday and today: Concrete of tomorrow. *Cem. Concr. Res.* **2000**, *30*, 1349–1359. [[CrossRef](#)]
4. Aydin, E. Novel coal bottom ash waste composites for sustainable construction. *Constr. Build. Mater.* **2016**, *124*, 582–588. [[CrossRef](#)]
5. Poudyal, L.; Adhikari, K. Environmental sustainability in cement industry: An integrated approach for green and economical cement production. *Resour. Environ. Sustain.* **2021**, *4*, 100024. [[CrossRef](#)]
6. Hwang, C.-L.; Huynh, T.-P. Engineering, Evaluation of the performance and microstructure of ecofriendly construction bricks made with fly ash and residual rice husk ash. *Adv. Mater. Sci. Eng.* **2015**, *2015*, 891412. [[CrossRef](#)]
7. Karim, M.; Zain, M.F.M.; Jamil, M.; Lai, F. Fabrication of a non-cement binder using slag, palm oil fuel ash and rice husk ash with sodium hydroxide. *Constr. Build. Mater.* **2013**, *49*, 894–902. [[CrossRef](#)]
8. Billong, N.; Melo, U.; Kamseu, E.; Kinuthia, J.; Njopwouo, D.J.C. Improving hydraulic properties of lime–rice husk ash (RHA) binders with metakaolin (MK). *Constr. Build. Mater.* **2011**, *25*, 2157–2161. [[CrossRef](#)]
9. Palomo, A.; Grutzeck, M.; Blanco, M. Alkali-activated fly ashes: A cement for the future. *Cem. Concr. Res.* **1999**, *29*, 1323–1329. [[CrossRef](#)]
10. Sun, Z.; Lin, X.; Vollpracht, A. Pervious concrete made of alkali activated slag and geopolymers. *Constr. Build. Mater.* **2018**, *189*, 797–803. [[CrossRef](#)]
11. Ariffin, M.; Bhutta, M.; Hussin, M.; Tahir, M.M.; Aziah, N. Sulfuric acid resistance of blended ash geopolymer concrete. *Constr. Build. Mater.* **2013**, *43*, 80–86. [[CrossRef](#)]
12. Ryu, G.S.; Lee, Y.B.; Koh, K.T.; Chung, Y.S. The mechanical properties of fly ash-based geopolymer concrete with alkaline activators. *Constr. Build. Mater.* **2013**, *47*, 409–418. [[CrossRef](#)]
13. Yurt, Ü. High performance cementless composites from alkali activated GGBFS. *Constr. Build. Mater.* **2020**, *264*, 120222. [[CrossRef](#)]
14. Rostami, M.; Behfarnia, K. The effect of silica fume on durability of alkali activated slag concrete. *Constr. Build. Mater.* **2017**, *134*, 262–268. [[CrossRef](#)]
15. Messina; Ferone; Colangelo; Roviello; Cioffi. Alkali activated waste fly ash as sustainable composite: Influence of curing and pozzolanic admixtures on the early-age physico-mechanical properties and residual strength after exposure at elevated temperature. *Compos. Part B Eng.* **2018**, *132*, 161–169. [[CrossRef](#)]
16. Van Deventer, J.S.; Provis, J.L.; Duxson, P. Technical and commercial progress in the adoption of geopolymer cement. *Miner. Eng.* **2012**, *29*, 89–104. [[CrossRef](#)]
17. Yang, K.-H.; Song, J.-K.; Song, K.-I. Assessment of CO<sub>2</sub> reduction of alkali-activated concrete. *J. Clean. Prod.* **2013**, *39*, 265–272. [[CrossRef](#)]
18. Fernandez-Jimenez, A.M.; Palomo, A.; Lopez-Hombrados, C. Engineering properties of alkali-activated fly ash concrete. *ACI Mater. J.* **2006**, *103*, 106.
19. Atiş, C.D.; Bilim, C.; Çelik, Ö.; Karahan, O. Influence of activator on the strength and drying shrinkage of alkali-activated slag mortar. *Constr. Build. Mater.* **2009**, *23*, 548–555. [[CrossRef](#)]
20. Palacios, M.; Puertas, F. Effect of carbonation on alkali-activated slag paste. *J. Am. Ceram. Soc.* **2006**, *89*, 3211–3221. [[CrossRef](#)]
21. Yum, W.S.; Suh, J.-I.; Sim, S.; Yoon, S.; Jun, Y.; Oh, J.E. Influence of calcium and sodium nitrate on the strength and reaction products of the CaO-activated GGBFS system. *Constr. Build. Mater.* **2019**, *215*, 839–848. [[CrossRef](#)]
22. Suh, J.-I.; Yum, W.S.; Jeong, Y.; Park, H.-G.; Oh, J.E. The cation-dependent effects of formate salt additives on the strength and microstructure of CaO-activated fly ash binders. *Constr. Build. Mater.* **2019**, *194*, 92–101. [[CrossRef](#)]
23. Kim, M.S.; Jun, Y.; Lee, C.; Oh, J.E. Use of CaO as an activator for producing a price-competitive non-cement structural binder using ground granulated blast furnace slag. *Cem. Concr. Res.* **2013**, *54*, 208–214. [[CrossRef](#)]
24. Yum, W.S.; Jeong, Y.; Yoon, S.; Jeon, D.; Jun, Y.; Oh, J.E. Effects of CaCl<sub>2</sub> on hydration and properties of lime (CaO)-activated slag/fly ash binder. *Cem. Concr. Compos.* **2017**, *84*, 111–123. [[CrossRef](#)]
25. Yum, W.S.; Suh, J.-I.; Jeon, D.; Oh, J.E. Strength enhancement of CaO-activated slag system through addition of calcium formate as a new auxiliary activator. *Cem. Concr. Compos.* **2020**, *109*, 103572. [[CrossRef](#)]
26. Jeon, D.; Yum, W.S.; Jeong, Y.; Oh, J.E. Properties of quicklime (CaO)-activated Class F fly ash with the use of CaCl<sub>2</sub>. *Cem. Concr. Res.* **2018**, *111*, 147–156. [[CrossRef](#)]
27. Mehta, P.K.; Monteiro, P.J. *Concrete Microstructure, Properties and Materials*; McGraw-Hill Education: New York, NY, USA, 2017.
28. Ministry of Land, I.T. Korea, *Korea Concrete Specification*; Ministry of Land: Daejeon, Korea, 2017.
29. Korean Standards Association. *Standard Test Method for Making Concrete Specimens*; KS F 2403; Korean Standards Association: Seoul, Korea, 2019.
30. Korean Standards Association. *Method of Test for Slump of Concrete*; KS F 2402; Korean Standards Association: Seoul, Korea, 2012.
31. Korean Standards Association. *Standard Test Method for Air Content of Fresh Concrete by the Pressure Method (Air Receiver Method)*; KS F 2421; Korean Standards Association: Seoul, Korea, 2011.
32. ACI Committee. *Building Code Requirements for Structural Concrete (ACI 318-08) and Commentary*; American Concrete Institute: Farmington Hills, MI, USA, 2008.

33. Comité Euro-International Du Béton. *CEB-FIP Model Code 1990, Design Code*; Institution of Civil Engineers Publishing: London, UK, 1993.
34. Korean Standards Association. *Standard Test Method for Resistance of Concrete to Rapid Freezing and Thawing*; KS F 2456; Korean Standards Association: Seoul, Korea, 2013.
35. ASTM. *Standard Test Methods for Chemical Resistance of Mortars, Grouts, and Monolithic Surfacing and Polymer Concretes*; ASTM C 267; ASTM: West Conshohocken, PA, USA, 2020.
36. Jeong, Y.; Park, H.; Jun, Y.; Jeong, J.-H.; Oh, J.E. Microstructural verification of the strength performance of ternary blended cement systems with high volumes of fly ash and GGBFS. *Constr. Build. Mater.* **2015**, *95*, 96–107. [[CrossRef](#)]
37. Ministry of Land, Infrastructure and Transport. *Korea, Concrete Standard Specification*; Korean Standards Association: Seoul, Korea, 2016.
38. Jo, B.-W.; Shon, Y.-H.; Kim, Y.-J. The evaluation of elastic modulus for steel fiber reinforced concrete. *Russ. J. Nondestruct. Test.* **2001**, *37*, 152–161. [[CrossRef](#)]
39. Kim, J.-K.; Han, S.H.; Song, Y.C. Effect of temperature and aging on the mechanical properties of concrete: Part I. Experimental results. *Cem. Concr. Res.* **2002**, *32*, 1087–1094. [[CrossRef](#)]
40. Alsalman, A.; Dang, C.N.; Prinz, G.S.; Hale, W.M. Evaluation of modulus of elasticity of ultra-high performance concrete. *Constr. Build. Mater.* **2017**, *153*, 918–928. [[CrossRef](#)]
41. Allahverdi, A.; Škvára, F. Acidic corrosion of hydrated cement based materials. *Ceram. Silikáty* **2000**, *44*, 152–160.
42. Shi, Z.; Geiker, M.R.; Lothenbach, B.; De Weerdt, K.; Garzón, S.F.; Enemark-Rasmussen, K.; Skibsted, J. Friedel's salt profiles from thermogravimetric analysis and thermodynamic modelling of Portland cement-based mortars exposed to sodium chloride solution. *Cem. Concr. Compos.* **2017**, *78*, 73–83. [[CrossRef](#)]
43. Goyal, S.; Kumar, M.; Sidhu, D.S.; Bhattacharjee, B. Resistance of mineral admixture concrete to acid attack. *J. Adv. Concr. Technol.* **2009**, *7*, 273–283. [[CrossRef](#)]
44. Roy, D.; Arjunan, P.; Silsbee, M. Effect of silica fume, metakaolin, and low-calcium fly ash on chemical resistance of concrete. *Cem. Concr. Res.* **2001**, *31*, 1809–1813. [[CrossRef](#)]
45. Taylor, H.F. *Cement Chemistry*; Thomas Telford: London, UK, 1997; Volume 2.
46. Scrivener, K.; Snellings, R.; Lothenbach, B. *A Practical Guide to Microstructural Analysis of Cementitious Materials*; CRC Press: Boca Raton, FL, USA, 2018.
47. Song, H.; Jeong, Y.; Bae, S.; Jun, Y.; Yoon, S.; Eun Oh, J. A study of thermal decomposition of phases in cementitious systems using HT-XRD and TG. *Constr. Build. Mater.* **2018**, *169*, 648–661. [[CrossRef](#)]
48. Bakharev, T.; Sanjayan, J.G.; Cheng, Y.-B. Resistance of alkali-activated slag concrete to acid attack. *Cem. Concr. Res.* **2003**, *33*, 1607–1611. [[CrossRef](#)]
49. Liu, X.; Feng, P.; Li, W.; Geng, G.; Huang, J.; Gao, Y.; Mu, S.; Hong, J. Effects of pH on the nano/micro structure of calcium silicate hydrate (CSH) under sulfate attack. *Cem. Concr. Res.* **2021**, *140*, 106306. [[CrossRef](#)]
50. Sverdrup, H.U. Calcite dissolution and acidification mitigation strategies. *Lake Reserv. Manag.* **1984**, *1*, 345–355. [[CrossRef](#)]
51. Pedrosa, E.T.; Fischer, C.; Morales, L.F.; Rohlfs, R.D.; Luttge, A. Influence of chemical zoning on sandstone calcite cement dissolution: The case of manganese and iron. *Chem. Geol.* **2021**, *559*, 119952. [[CrossRef](#)]
52. Feng, P.; Miao, C.; Bullard, J.W. A model of phase stability, microstructure and properties during leaching of portland cement binders. *Cem. Concr. Compos.* **2014**, *49*, 9–19. [[CrossRef](#)]